iScience

CellPress
OPEN ACCESS

Article

A global North-South division line for portraying urban development

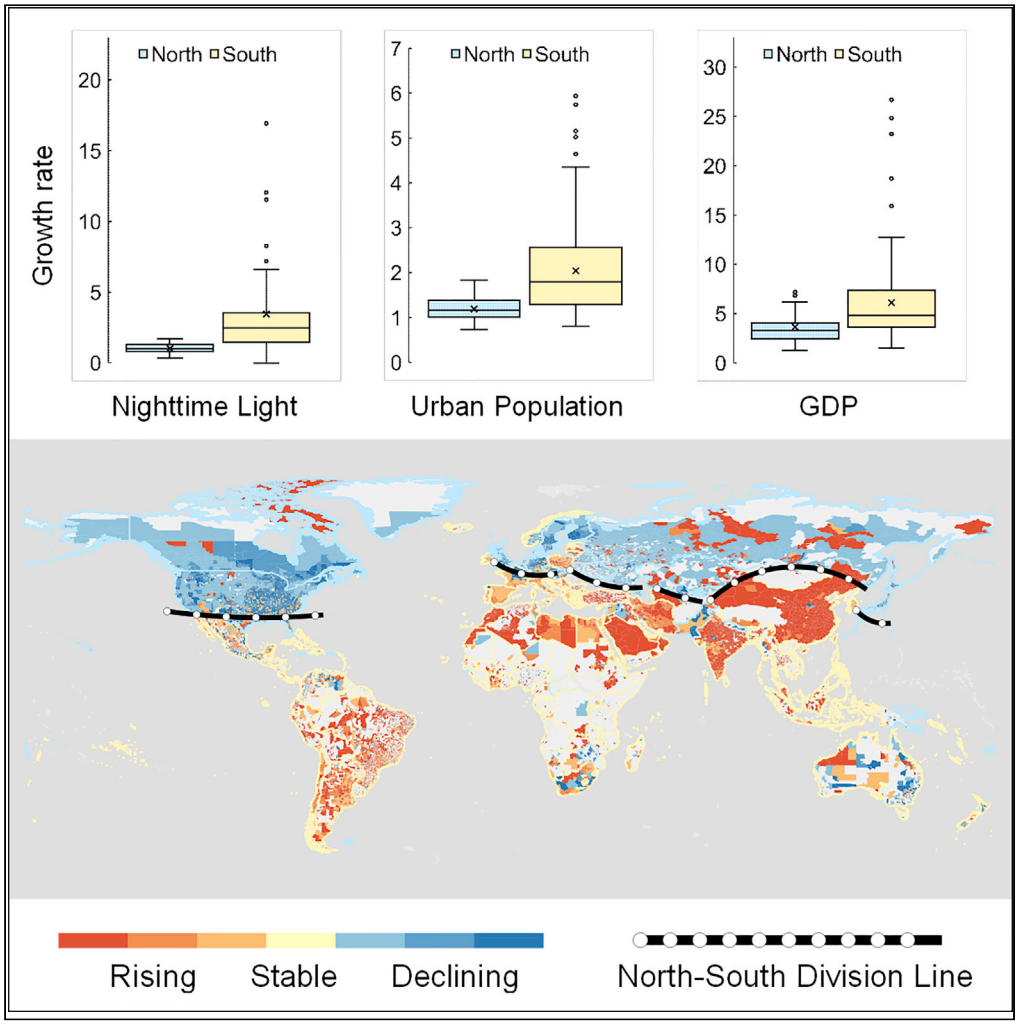

Yatao Zhang, Xia Li, Shaojian Wang, ..., Kuishuang Feng, Laixiang Sun, Klaus Hubacek

lixia@geo.ecnu.edu.cn (X.L.)
wangshj8@mail.sysu.edu.cn (S.W.)
k.hubacek@rug.nl (K.H.)

Highlights

Nighttime light performs well in measuring global urban development at multi-scales

A North-South division line splits global urban development patterns geographically

The socioeconomic difference accords with the proposed North-South division line

The North-South division line may keep stable but also bears uncertainties

Zhang et al., iScience *24*, 102729
July 23, 2021
https://doi.org/10.1016/j.isci.2021.102729

iScience

CellPress
OPEN ACCESS

Article

A global North-South division line for portraying urban development

Yatao Zhang,[1,12] Xia Li,[2,12,*] Shaojian Wang,[3,4,*] Yao Yao,[5] Qingquan Li,[6,7] Wei Tu,[6] Hongfang Zhao,[2] Hui Zhao,[8] Kuishuang Feng,[9] Laixiang Sun,[9] and Klaus Hubacek[10,*]

SUMMARY

Rapid urbanization has tremendously changed the global landscape with profound impacts on our society. Nighttime light (NTL) data can provide valuable information about human activities and socioeconomic conditions thus has become an effective proxy to measure urban development. By using NTL-derived urban measures from 1992 to 2018, we analyzed the spatiotemporal patterns of global urban development from country to region to city scales, which presented a distinct North-South divergence characterized by the rising and declining patterns. A global North-South division line was identified to partition the globe into the Line-North and the Line-South geographically, which accorded with the socioeconomic difference from the aspects of urban population and economy. This line may keep a certain degree of stability deriving from the trends of population and economic information but also bears uncertainties in the long term.

INTRODUCTION

In 2007, the global urban population surpassed the global rural population for the first time in history (UN DESA, 2018), although only about 0.5% of global land can be classified as urban areas (Zhou et al., 2015). The share of the global population living in cities had experienced a huge increase from about 42.9% in 1990 to 54.0% in 2014 and was estimated to reach about 66.0% in 2050 (UN DESA, 2018), reflecting the rapid growth of global urbanization (Buhaug and Urdal, 2013). Under these circumstances, global urban development exerts considerable impacts on a range of aspects with the pros and cons, such as influencing global economic growth in agriculture, manufacturing, and service sectors (Messinis, 2015), and imposing health problems (Eckert and Kohler, 2014). Also, it is linked to an increased risk of social disruption (Buhaug and Urdal, 2013) and directly contributing to declining biodiversity and fragile ecological environments (McDonald et al., 2013). Therefore, deeply exploring the spatiotemporal patterns of global urban development is significant to understand the international situation and evaluate its potential variations and can provide effective references for handling challenges from social, economic, and environmental issues to ensure a sustainable future.

Inspired by the sustainable development goals (SDGs), the global urban agenda presented an obvious characteristic that determined the importance of cities for sustainable development and has achieved broad agreement of a New Urban Agenda across a majority of countries (Parnell, 2016). The agenda underlined the centrality of an urban perspective in realizing national and international development in a sustainable way (Acuto et al., 2018). Theoretically, global urban studies have generated a series of concepts and analytical methodologies, such as comparative imaginations (Robinson, 2011, 2016), planetary urbanization (Merrifield, 2013; Oswin, 2018), urban assemblages (Far I As and Bender, 2012; McFarlane, 2011), and worlding cities (Connolly, 2019; Roy and Ong, 2011). These studies are aimed at proposing a more global urban approach to understanding cities although more work is still under way (Robinson, 2016). However, stepping into the new urban era, existing urban theories are no longer sufficient to support global sustainability from a comprehensive view, thus creates the necessity of building a global urban science to directly link science to practice (Acuto et al., 2018). Correspondingly, the SDGs has begun to put forward requirements for a data-driven technological revolution in urban development practices (Parnell, 2016), referring to the greater acceptance of geospatial big data to explore global urban studies.

Traditionally, limited by two main aspects, most existing studies only focused on a subset of the world's cities, rather than analyzing urban development at the global level (Cohen, 2006; Small et al., 2011; Wang

[1]Future Resilient Systems, Singapore-ETH Centre, ETH Zurich, Singapore 138602, Singapore

[2]School of Geographic Sciences, Key Lab of Geographic Information Science (Ministry of Education), East China Normal University, Shanghai 200241, China

[3]School of Geography and Planning, Guangdong Provincial Key Laboratory of Urbanization and Geo-simulation, Sun Yat-sen University, Guangzhou 510275, China

[4]Department of Urban Studies and Planning, Massachusetts Institute of Technology, Cambridge, MA 02139, USA

[5]School of Geography and Information Engineering, China University of Geosciences, Wuhan 430078, China

[6]Shenzhen Key Lab of Spatial Smart Sensing and Services, Key Lab for Geo-Environmental Monitoring of Coastal Zone of the Ministry of Natural Resource, Shenzhen University, Shenzhen 518060, China

[7]State Key Laboratory of Information Engineering in Surveying, Mapping and Remote Sensing, Wuhan University, Wuhan 430079, China

[8]Guangdong Urban and Rural Planning and Design Institute Co. Ltd., Guangzhou 510290, China

[9]Department of Geographical Sciences, University of Maryland, College Park, MD 20742, USA

[10]Integrated Research of Energy, Environment and Society (IREES), Energy and Sustainability Research Institute (ESRIG), University of

Continued

et al., 2012; Zhang and Seto, 2011): (i) There is a lack of agreement on how to measure urban development with a global standard (Cohen, 2006; Small et al., 2011). Taking the ratio of urban population to the total population as an example, which is a prevalent indicator used in the *World urbanization prospects* (UN DESA, 2018), there may exist quite major errors and some degree of uncertainty (Cohen, 2004, 2006). Moreover, how to define the term, urban population, could vary globally, such as identifying urban communities by population size or density, economic functions, administrative boundaries, etc (Cohen, 2006). (ii) The other is a barrier to obtain consistent and reliable data to monitor global urban development at fine spatial and temporal scales (Zhang and Seto, 2011; Zhou et al., 2014). Although satellite images can provide available data sources to observe urban variations, it is difficult to access temporally consistent global land-use products (Li et al., 2017a; Zhang and Seto, 2011). Statistical data obtained from some international institutions, such as the United Nations and the World Bank, frequently fail to provide information on the distribution and extent of the urban environment (Zhang and Seto, 2011). At the same time, data collection capabilities at the local level are frequently underdeveloped and dysfunctional for many regions unable to collect effective urban data (Acuto and Parnell, 2016).

To fill the void, there have been many studies to explore the global urban extent and its expansion process by using remotely sensed technologies (Seto et al., 2011), such as NTL data, MODIS, Landsat and SAR. In detail, Zhou et al. (2015) created a global 1km urban extent map by utilizing NTL data; Schneider et al. (2009) produced a map of the global urban area with a spatial resolution of 500 m based on MODIS data; Gong et al. (2013) utilized Landsat images and Google Earth tools to generate 30 m resolution global land-cover maps; Esch et al. (2017) provided a map of global urban and rural settlements with about 12 m resolution by using TanDEM-X and TerraSAR-X radar images. Similar studies can also be found to portray global urban extent (Ban et al., 2015; Sharma et al., 2016; Zhou et al., 2014), but the problem is that these studies only focused on one particular year, which limits the ability to monitor global urban expansion from a long-term perspective. This problem also exists in widely used global land-use products, such as GlobeLand30 and GlobCover 2009 (Gong et al., 2013; Jokar Arsanjani, 2019). Among all these remote sensing images, NTL has the greatest potential to monitor global urban development from a time-series perspective, such as some studies that explored global urban dynamics covering a long time period (Chen et al., 2019b; Zhang and Seto, 2011; Zhou et al., 2018).

NTL data can collect light and its intensity generated by most human settlements in the world (Elvidge et al., 2009), which has the potential to measure the degree of urban development and explore the spatiotemporal variations of human activities (Zhou et al., 2014, 2015). As a proxy of urban development, it reflects the process of urbanization involving the combined effect of changes in demographic compositions, economic activities, and land use (Zhang and Seto, 2011). Many studies have demonstrated the usefulness of NTL to monitor urban development globally and explored the quantitative relationship between time-series NTL data and various aspects, such as socioeconomic, environmental, and energy-related factors (Li and Zhou, 2017; Ma et al., 2012; Proville et al., 2017; Sutton et al., 2001; Yu et al., 2018; Zhang and Seto, 2011). Moreover, compared with urban population obtained from statistical agencies and other sources, utilizing the NTL data to monitor global urban development has the following advantages: (i) it can monitor urban areas at any acquired spatial scales from its minimal spatial resolution to a near-global coverage (Zhou et al., 2015); (ii) it covers a long temporal coverage from 1992 to the present and the future; (iii) its intensity can depict both the spatial and temporal variations within cities; (iv) it avoids the necessity to unify the definitions of urban population across countries; (v) it can reflect the urban development from demography, economy and land use simultaneously (Ma et al., 2012), thus making it more comprehensive as the urban measure.

In this study, we unified the global standard of urban development as the NTL-derived urban measure to detect its spatiotemporal patterns from 1992 to 2018. Three scales were first established to exhibit the comprehensive portrayal of global urbanization based on the Global Administrative Areas dataset (GADM) (Global Administrative Areas, 2015), i.e., country-scale, region-scale (provinces or states) and city-scale. Then, time-series NTL-derived urban measures were generated at the three scales after eliminating light deviations (Ma et al., 2012), inter-calibrating light data from different sensors (Elvidge et al., 2009; Li et al., 2017b) and filtering noises of NTL data. We then drew multi-scale pattern maps of global urban development to present its spatiotemporal patterns through the shape-based clustering method and the reclassification method. Finally, this study explored the global socioeconomic difference and evaluated its potential variations.

Groningen, Groningen, 9747 AG, the Netherlands

[12]These authors contributed equally

*Correspondence: lixia@geo.ecnu.edu.cn (X.L.), wangshj8@mail.sysu.edu.cn (S.W.), k.hubacek@rug.nl (K.H.)

https://doi.org/10.1016/j.isci.2021.102729

RESULTS

Temporal patterns of global urban development

We used the shape-based clustering method to analyze the shape variations hidden behind time-series NTL vectors and extracted the temporal patterns of global urban development during the period of 1992-2018 at the country, region, and city scales (Berndt and Clifford, 1994; Elvidge et al., 2014). The Silhouette scores provide an evaluation of the clustering quality with various cluster numbers (Rousseeuw, 1987) (middle charts in Figure 1). A higher Silhouette score means a better clustering result. The highest Silhouette scores are obtained when the cluster number is two at all three scales, indicating that the clustering quality is the best at this point. The temporal curves exhibit the shape patterns of each cluster through the two clustering center curves (left charts in Figure 1).

At all three scales, we find that the clustering center curve in yellow acts as an overall rising trend in which temporal variations of NTL-derived urban measures gradually increase along time if ignoring local fluctuations, namely the rising pattern. In contrast, the clustering center curve in blue shows an overall declining trend in which NTL-derived urban measures gradually decrease along the horizontal axis regardless of local fluctuations, namely the declining pattern. The rising and declining trends endow urban development patterns with two opposite states by simultaneously interpreting their temporal variations. In detail, compared to areas with the rising pattern, the urban development process of areas with the declining pattern slackened relatively during the period, and it was not equivalent to that the latter's urban development reduced at each temporal moment. Also, as the NTL data holds a close relationship with socioeconomic factors, such as urban population, economic conditions, and land use (Ma et al., 2012; Zhang and Seto, 2011), the rising and declining patterns can reflect temporal variations on the combined effect of underlying factors that contribute to the observable urban development by NTL data, without the consideration of specific underlying interactions among these factors.

Spatial patterns of global urban development

We find that these countries have the clustered phenomenon in the spatial distribution of rising and declining through the measurement of spatial autocorrelation by the Global Moran's I (maps in Figure 1). Given the geometric features and their associated attributes, the Moran's I is utilized to evaluate whether the spatial pattern is random, clustered (Moran's $I > 0$) or dispersed (Moran's $I < 0$), while the Z score and p value can evaluate its significance (Getis, 2010). For areas with extremely low NTL-derived urban measures, they were listed as excluded areas with large numbers at the region and city scales. Their spatial distribution is also clustered, mainly located in Africa, Latin America, and Asia.

At the country scale, the Moran's I is statistically positive in terms of the spatial autocorrelation (Moran's $I = 0.15$, Z score $= 5.75$, p value < 0.01). Many countries with the rising pattern are spatially clustered together south of the globe, whereas countries with the declining pattern are mainly spatially clustered north of the globe. At the region scale, the statistically positive Moran's I implies the clustered patterns of the spatial distribution of the two temporal patterns too (Moran's $I = 0.30$, Z score $= 85.87$, p value < 0.01). Most regions hold the same temporal patterns as the countries they belong to. Also, there exist some exceptions, such as regions in Africa and Oceania, which mostly have relatively low NTL-derived urban measures. Thus, their actual temporal patterns are hidden and not present at the country scale. At the city scale, we also get a statistically positive Moran's I again (Moran's $I = 0.33$, Z score $= 655.95$, p value < 0.01). After excluding the areas with extremely low NTL-derived urban measures, the cities in close proximity with the same temporal patterns can be aggregated into area agglomerations. For example, cities aggregated in China, India, and Latin America are such agglomerations with the rising pattern (yellow area in Figure 1C); cities aggregated in North America, Europe, and Japan constitute such agglomerations with the declining pattern (blue area in Figure 1C).

A North-South division line of global urban development

We find that there exists a pronounced North-South difference in the spatiotemporal patterns of urban development across the globe, which can be generally divided by a latitudinal line (white-black belts in Figure 1). This line leans close to the boundaries of America, England, Germany, Russia, China, Japan, etc. Here, this line is defined as a North-South division line, which provides a geographical division of the temporal and spatial patterns of global urban development. The patterns above and below the division line are generally opposite, with the temporal declining pattern in the Line-North and the temporal rising pattern in

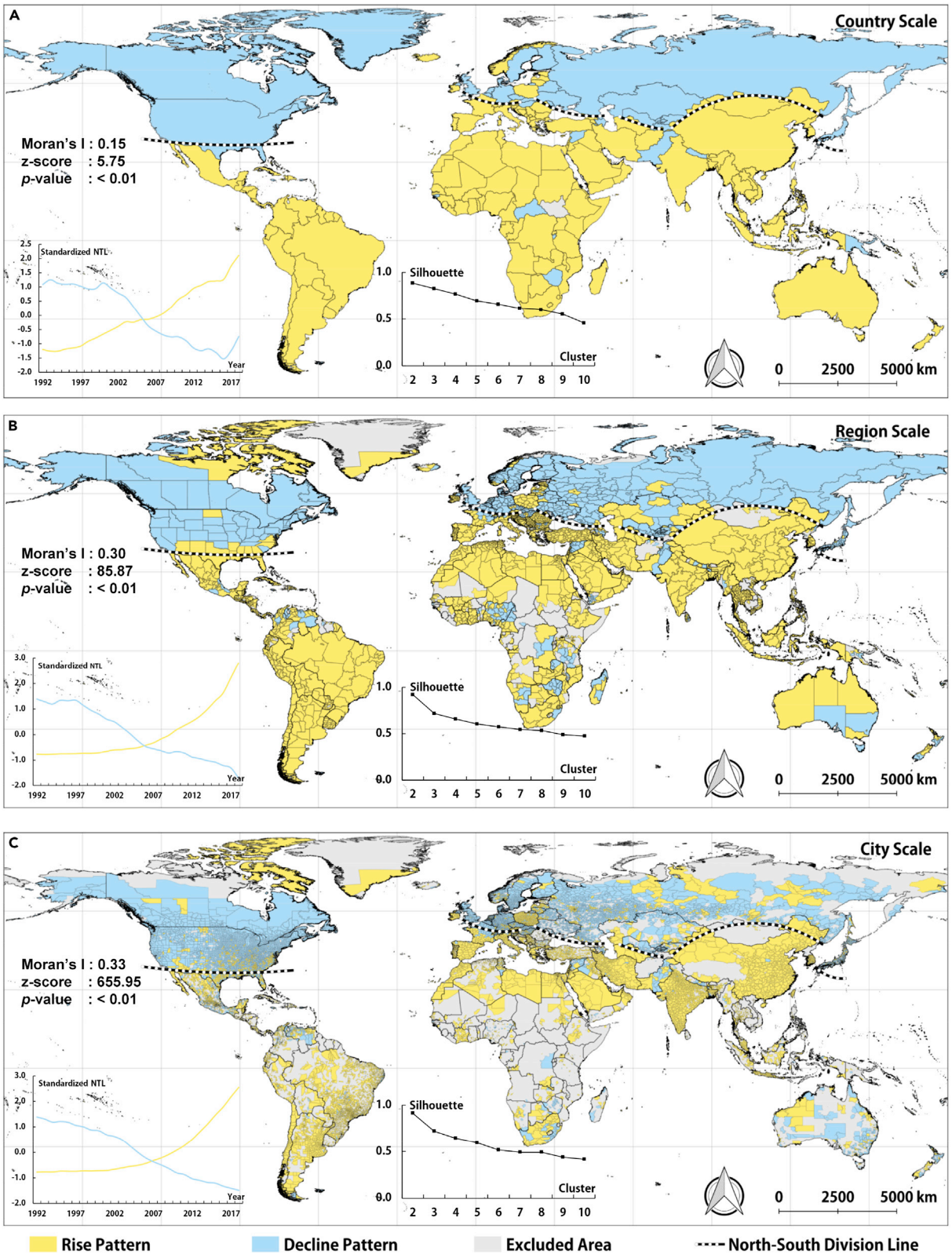
A
Country Scale
Moran's I : 0.15
z-score : 5.75
p-value : < 0.01
Standardized NTL
Year
Silhouette
Cluster
0 2500 5000 km
B
Region Scale
Moran's I : 0.30
z-score : 85.87
p-value : < 0.01
Standardized NTL
Year
Silhouette
Cluster
0 2500 5000 km
C
City Scale
Moran's I : 0.33
z-score : 655.95
p-value : < 0.01
Standardized NTL
Year
Silhouette
Cluster
0 2500 5000 km
Rise Pattern
Decline Pattern
Excluded Area
North-South Division Line

Figure 1. Spatiotemporal patterns of global urban development and its North-South division line

(A) Country scale.

(B) Region scale.

(C) City scale. Every subfigure consists of four elements: the middle chart depicts the varying Silhouette scores as the number of clusters increases; the left chart provides the clustering center curves with the highest Silhouette score, where the yellow and blue curves present the shape variations of the temporal rising and declining patterns respectively; the map exhibits the spatial distribution of two patterns, with a North-South division line across it, and excluded area refers to the units with extremely low NTL-derived urban measures; the Global Moran's I and its p-value give the measurement of the spatial autocorrelation regarding two patterns.

the Line-South. An interesting phenomenon is that most high-income countries are located in the Line-North, such as countries in North America, Western and Northern Europe; while most rapidly developing, lower-middle-income and low-income countries lie in the Line-South, such as countries in Asia, Latin America and Africa. This implies a possible relationship between the North-South division line and the socioeconomic conditions of these countries.

The North-South division line can take effects on partitioning the spatiotemporal patterns of global urban development at all three scales. However, it does not mean to strictly divide the globe into two parts with the opposite patterns, but to provide the general geographical difference of the two temporal patterns. Thus, some cities could hold the declining pattern different from most areas in the Line-South, such as cities in Africa. Moreover, although the administrative units become fragmented with the refinement of spatial scales, the difference in the two parts produced by the North-South division line is still pronounced. Meanwhile, the fragmented distribution can provide interesting details of the local difference in spatiotemporal patterns of urban development within countries, such as cities in Russia.

Spatial heterogeneity of urban development in the Line-South and the Line-North

To explore the difference in the two parts produced by the North-South division line in detail, we provide a finer portrayal of global urban development based on the change rate of the temporal rising and declining trends at the city scale. The temporal patterns of urban development are reclassified into seven types, including a stable pattern (constant in NTL-derived urban measures), three rising patterns (accelerated, uniform and decelerated) and three declining patterns (accelerated, uniform, and decelerated). They are schematically matched to the standard curves in the left diagram of Figure 2A. The map in Figure 2A shows that after introducing the stable patterns, the geographical distribution of cities with the temporal rising and declining patterns is still generally aligned with the North-South division line. Moreover, the number of cities listed as the excluded area (extremely low NTL-derived urban measures) accounts for nearly 46.88%, indicating that there exists a huge gap in the process of global urban development. In the following, we explore several cases in the Line-South and the Line-North to demonstrate the difference in urban development and its patterns.

In the Line-South, as the two largest developing countries, the patterns of urban development in China and India show significant differences (Figures 2B and 2C). First, the patterns of Chinese cities are more geographically and quantitatively homogeneous than those of India. More than 89.29% of Chinese cities fall into the temporal rising pattern that are evenly distributed across the vast territory of China. But its proportion in India is about 79.88%, and such distribution is interrupted by cities with the temporal declining pattern and excluded areas. Second, China held a much stronger urbanized pattern than India during the period of 1992-2018. Cities with the accelerated rise pattern in China account for 76.79%, and there is only about 1.79% with the declining pattern, whereas these shares in India are 58.41% and 3.45%, respectively (Table S1). Although both countries implemented economic reforms and underwent rapid urbanization in the past decades, China's urban development was more rapid (Bosworth and Collins, 2008). Also, their economic growth trends were quite different, with China showing more growth in industrial production, whereas India showing more growth in the service sector (Sankhe et al., 2011).

In the Line-North, the United States and Japan produce great differences in the patterns of urban development (Figures 2D and 2E). First, the composition of their patterns varies a lot. Although they both hold small proportions in cities with the temporal rising pattern, cities in the US with the temporal declining pattern account for 78.02%, whereas this share in Japan is only 55.33%, and the stable pattern raises to 22.53% (Table S1). Second, there exist great differences in the distribution of cities with the temporal rising pattern. In Japan, lots of cities with the rising pattern concentrate in the three biggest metropolitan areas,

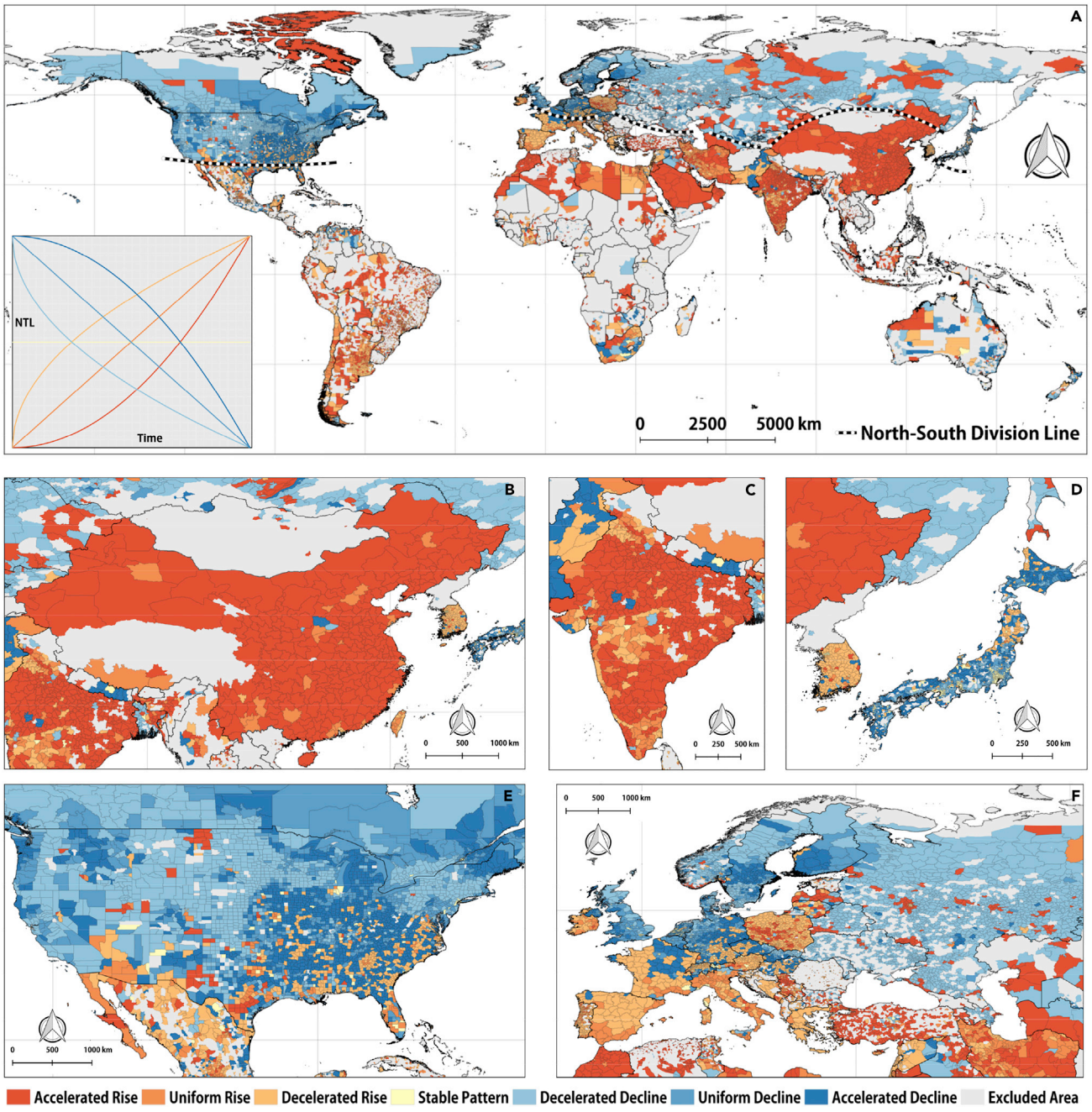

Figure 2. Finer patterns of urban development and the local enlarged maps

(A) A global map for finer patterns of urban development. The left chart illustrates a schematic diagram of different patterns considering the change rate of the rising and declining patterns (using simulated data).

(B) The main area of China. (C) The main area of India. (D) The main area of Japan. (E) The main area of the United States. (F) The main area of Europe. Note that (B-F) are the enlarged maps of (A).

including Kantō, Keihanshin, and Chūkyō. In the US, cities with the temporal rising pattern are mostly scattered in the southeast, south, and southwest, such as metropolitan Atlanta, Dalla-Fort Worth and Phoenix, which present a nebular spatial clustering feature. This can be explained by the fact that urbanization in the Southern United States happened much later than the Northeastern and Midwestern United States (Lloyd, 2012; Pandit, 1997). While in Japan, the population was extremely concentrated in the metropolitan areas, and the population density descended sharply in small towns (Bagan and Yamagata, 2012, 2015).

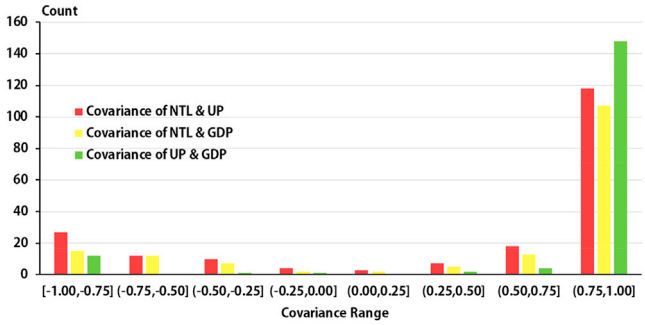

Figure 3. Mutual covariances among nighttime light derived urban measures (NTL), urban population (UP) and gross domestic product (GDP) at the country scale

Before calculating the covariance, time-series UP and GDP data were processed by the exponential smoothing method and *Z* score standardization to accord with NTL. Note that the covariance is calculated only for countries with no missing data of two factors.

In Europe, where the division line crosses, the patterns' distribution of urban development presents a quite complicated situation, which is closely related to its historical origins (Figure 2F). European cities had experienced the urbanization evolution at different speeds and time historically, thus leading to wide disparities in the urban development between Northern and Southern Europe (Antrop, 2004; Cheshire, 1995), which can be observed above and below the division line in the period of 1992-2018 (Figure 2F). However, the difference of European patterns is not only between Northern and Southern Europe, but it is also shown between Western and Eastern Europe (Turok and Mykhnenko, 2007). In the 1990s, events such as the dissolution of the Soviet Union, the revolution of 1989, and the unification of Germany produced profound influences on European demography and economy (Judt, 2006), which in turn affected its urban development. Many cities in Eastern Europe are dominated by the temporal declining pattern (Figure 2F), such as cities in Czechia, Slovakia, and Ukraine. Similarly, cities in European Russia mostly hold the temporal declining pattern, with only a few agglomerations in the temporal pattern, like areas surrounding Moscow. Moreover, many cities in Western Europe also hold the temporal declining pattern, such as the UK and West Germany, but the difference is that these cities mostly had experienced a big step in urban development before 1990 influenced by historical and political factors.

Socioeconomic differences between the Line-South and the Line-North

Urban development is a complex process involving multiple socioeconomic factors (Ma et al., 2012; Zhang and Seto, 2011). Then one question arises of what is the relationship between the NTL-derived urban measure and various socioeconomic factors. Can these socioeconomic factors be related to the North-South division line? Taking the eastern coastal area of China as an example, the Pearson's R shown in Table S2 illustrates the close correlation between the NTL-derived urban measure and socioeconomic factors from the perspective of demography, economy, and land use at three scales.

In order to explore this relationship globally, we specially selected urban population and GDP to compute their mutual covariance and the covariance with the NTL-derived urban measure from 1992 to 2018 at the country scale. In Figure 3, the majority of countries are situated in the range of (0.75, 1.00) and few countries are in the range of (0.00, 0.75) regarding their mutual covariance, revealing the positive correlation among NTL, GDP, and urban population. However, there are some interesting outliers, such as Romania where the covariance of GDP and urban population is negative, but the covariance of GDP and NTL is positive; whereas in Russia we find a negative relationship between NTL and GDP but a positive relationship between NTL and urban population. It leads to a contradiction that it is not adequate to monitor global urbanization by only using population and economic growth. It also emphasizes the importance of introducing the NTL-derived urban measure.

Based on the above analysis, we need to further explore what is the socioeconomic difference between the Line-South and the Line-North by utilizing these interesting factors. Here, the growth rates of the NTL-derived urban measure, urban population and GDP between 1992 and 2018 were calculated to compare their spatial variations at the country scale. As shown in Figure 4A, the spatial distribution of NTL's growth rate is highly consistent with the North-South division line, with an apparently higher rate of the Line-South

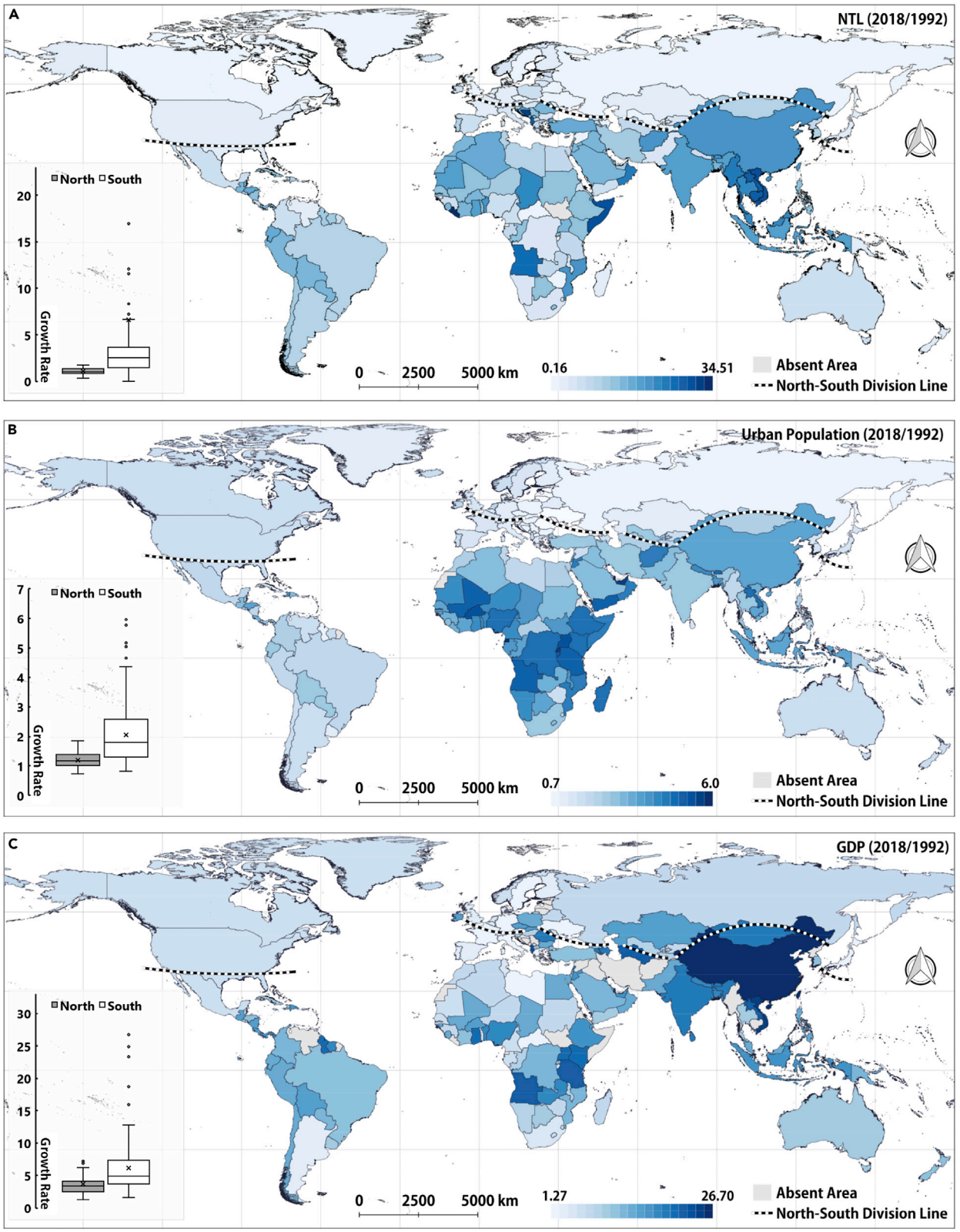
A
NTL (2018/1992)
North South
Growth Rate
0 5 10 15 20
0 2500 5000 km
0.16
34.51
Absent Area
North-South Division Line
B
Urban Population (2018/1992)
North South
Growth Rate
0 1 2 3 4 5 6 7
0 2500 5000 km
0.7
6.0
Absent Area
North-South Division Line
C
GDP (2018/1992)
North South
Growth Rate
0 5 10 15 20 25 30
0 2500 5000 km
1.27
26.70
Absent Area
North-South Division Line

Figure 4. Growth rate maps (2018/1992) of global socioeconomic factors and box plots in the Line-North and the Line-South

(A) nighttime light derived urban measures (NTL).

(B) Urban population.

(C) Gross domestic product (GDP). The box plot in each subfigure presents the data distribution of growth rates of the socioeconomic factor in the Line-North and the Line-South. Meanwhile, due to the lack of data (World Bank) in some countries, we list them as the absent area in the maps and exclude them from the calculations in the box plots.

than that of the Line-North. Similarly, the socioeconomic factors (urban population and GDP) also exhibit a huge divergence on both spatial distributions and growth rates above and below the division line in Figures 4B and 4C, i.e., the Line-South greater than the Line-North. Considering that the NTL-derived urban measure is closely related to urban population and GDP simultaneously, it can provide assistance to portray the socioeconomic difference globally.

In terms of urban population, the growth pole concentrates on Asia and Africa shown in Figure 4B. Its distribution is similar to the spatial agglomeration of NTL's growth rate in Figure 4A, despite the larger NTL's growth rate of Asia than Africa compared to the growth rate of urban population. The overall growth rate in Latin America is a little higher than that of North America. In Europe, although the demographic difference of the growth rates above and below the line is not obvious, there is a wide divergence above and below the Mediterranean Sea. It seems that although the division line crosses Europe, the change trend of urban population within European countries is still fairly similar on a global scale. Moreover, from the box plot in Figure 4B, the range of urban population growth in the Line-North is less spread with an average growth rate of 1.19, while the average value in the Line-South is much higher, i.e., 2.04. It is highly consistent with the *World urbanization prospects*, e.g., Asia and Africa are urbanizing faster than other regions and will maintain this situation in the coming decades (UN DESA, 2018).

In terms of the economic indicator, GDP's growth rate is significantly different between the Line-South and the Line-North shown in Figure 4C. The growth pole of GDP also concentrates on Asia and Africa, and GDP's growth is more obvious in Asian countries rather than African countries. This is similar to the spatial distribution of NTL's growth rate in these countries. Compared with urban population, the distribution of GDP's growth rate in the Americas and Europe has more similarities to that of NTL. For example, the difference in GDP's growth rate for different countries above and below the line is apparent in the Americas. From Mexico to Argentina, the countries in Latin America hold higher economic growth than those in the United States and Canada. In Europe, this similarity is embodied in countries along the northeast coast of the Mediterranean Sea. Moreover, the extent of economic growth is notably larger than that of urban population, whose average growth rates have achieved 3.69 and 6.01 for countries on the two sides of the division line from 1992 to 2018, respectively. For several countries in the Line-South, the growth rate of these years is even over 20, e.g., China.

Furthermore, many countries with low levels of GDP have displayed a trend of higher growth rates. For instance, almost all countries in Africa present low-level absolute values about the NTL-derived urban measure, urban population and GDP in Figure S1, but their values of the growth rate are much higher than many other countries in Figure 4. In contrast, many countries with high-level GDP possess low-level growth rates, especially in Western Europe and North America, which are a reflection of their development stages. This phenomenon to some extent implies that the latter had experienced a huge economic lead before the 1990s and would be in a relatively slow state of economic growth, whereas many countries with low levels of GDP are and would continue to be in the rapid growth of urban development (Dellink et al., 2017; Maddison, 1983). In this process, international cooperation and technical upgrade could be important to promote economic growth in African and Southeast Asian countries, and thus can greatly benefit the process of urban development. In addition, some rapidly developing countries have both high absolute values and growth rates of the NTL-derived urban measure, urban population and GDP simultaneously, e.g., China and India. The relatively low per capita income will continue to stimulate these two countries to maintain high economic growth in the near future.

Generally, the NTL-derived urban measure can reflect the socioeconomic difference through its close relationship with urban population and GDP, thus endowing it the ability to monitor urban development comprehensively with a global standard (Ma et al., 2012; Zhang and Seto, 2011). It is gradually becoming a useful proxy of urbanization and provide rich connotations of urban development at a large scale.

DISCUSSION

Detecting the spatiotemporal patterns of global urban development is of great significance to understand current international situations and their potential variations. The North-South division line proposed here reminds us of the old North-South divide concerned with politics and poverty in the 20th century (Therien, 1999). But the division line mainly aims at revealing the spatiotemporal distributions and patterns of global urban development during the period of 1992-2018, without the involvement of politics, etc. In essence, the characteristic of the North-South division line is conceptually similar to that of China's Hu-Huanyong Line, which divides the area of China into two roughly equal parts with different patterns of urban development (Chen et al., 2019a). Thus, it should be more appropriate to analogize this division line to the Hu's line on a global scale. The meaning of identifying such a division line is not limited to revealing its geographical patterns but also exploring how to understand global issues based on this line and other auxiliary information, related to the population and economy.

Owing to higher fertility rates and larger shares of young age groups, the areas in the Line-South would have larger population growth than that in the Line-North. Many countries in the Line-North have shown an aging population reflecting a long-term population transformation, but this process just began in many countries of the Line-South (Higo and Khan, 2015). In the population forecast for 2100, most countries in Africa, Middle East, India and Southeast Asia would present a rapid growth, while European and North American countries and Japan would have population decline in various projected scenarios (Jones and O Neill, 2016). One major challenge caused by the aging population is the decrease in labor supply, which could exert significant impacts on economic development and burdening the working population (Bloom et al., 2015). In the past three decades, GDP's growth rate in the Line-South was much larger than that of the Line-North in spite of reverse absolute GDP values. Further, in the projected scenarios of shared socioeconomic pathways which satisfy the conditional convergence hypothesis, countries in the Line-South would generally keep a long-term higher growth rate of GDP than that of the Line-North in the 21st century because of the catch-up effect in key drivers of economic development (Dellink et al., 2017).

The long-term trends of population and economic growth imply that urban development in the Line-South has a high chance to grow faster than the Line-North and keep the rising pattern. Similar to China's Hu-Huanyong Line that is hard to break, the global North-South division line also shows a sign of being relatively stable deriving from population and economic transformations for a long period. However, multifarious development scenarios and external influencing factors would exert unpredictable impacts on global economic growth (Dellink et al., 2017), making the assessment of long-term trends of urban development complicated and uncertain. For instance, due to serious population aging in the next several decades, China may experience a substantial total population decline and the potential lack of labor force (Higo and Khan, 2015; Jones and O Neill, 2016), which could result in a southward shift of the North-South division line in Asia gradually. Furthermore, another timely example is negative influences on the global economic growth caused by the COVID-19 (Fernandes, 2020), especially the regions with high dependence on tourism, e.g., the Caribbean and some countries with a dominating sector, and the regions with massive amount of confirmed cases, e.g., the United States. The point is that such major events will also deeply affect international cooperation and employment, contributing to a higher degree of uncertainty regarding global urban development.

In addition, global urban development is to assert significant impacts on environmental issues, which require particular attention to ensure a sustainable future. In the process of economic growth and global urbanization, carbon emissions increased rapidly and would continue to grow in the next several decades despite recent declines in emissions due to COVID-19 (Le Quere et al., 2020; O'Neill et al., 2010). While a number of rich countries in the Line-North have achieved some level of decoupling of emissions from economic growth, albeit at a very high level of per capita carbon footprints; many countries in the Line-South are bound to further increase carbon emissions due to development goals and rapid industrialization. These countries would undoubtedly meet great challenges to balance environmental protection and urban development.

Methodologically, the hierarchical portrayals of global urbanization from country to city scales provide a comprehensive understanding to detect the spatiotemporal patterns of urban development and reveal the applicability of the North-South division line in multi-scenarios. Also, the approach introduces a new perspective involving various scales into the analysis of global urban development, which can be extended to other research of large-scale geographical phenomenon and explore their intrinsic characteristics at

different time and space granularities. The NTL data used in this study presents its great potentials to draw global urban maps and uncover the spatiotemporal variations of urbanization due to its wide coverage and continuity, and it can be developed as a globally unified definition for urban development at any acquired scales. In addition, this study takes full use of the association between NTL-derived urban measures and various socioeconomic indicators to disclose the difference in the growth variations of population and economy between the Line-North and the Line-South, which is of great importance to understand global issues.

Conclusion

In the research of global urbanization processes, it is challenging to comprehensively describe urban development and detect its spatiotemporal variations. This study utilized NTL data to explore development patterns of global urbanization due to its low cost, wide spatiotemporal coverage, and rich connotations of human activities. At the same time, its close correlation with demographic and economic factors can provide important reference points to understand global issues.

In this study, we find that the spatiotemporal patterns of global urban development present a North-South divergence characterized by rising and declining trends, which can be geographically partitioned by the latitudinal North-South division line. This line exhibits geographical differences in global urban development during the period of 1992-2018: countries in the Line-South show a higher rapid economic growth and are likely to continue this trend, whereas countries in the Line-North show lower economic growth rates. The city-scale reclassification reveals that there are also huge differences in the patterns of urban development on the same side of the line, e.g., China and India, the United States and Japan.

Furthermore, the North-South division line would maintain a certain degree of stability due to the potential long-term trends of population and economy, but it is still difficult to provide accurate projections about its future variations. The meaning of identifying this division line is not only to reflect the spatiotemporal distributions but also to help understand international socioeconomic dimensions. To some extent, the Hu-Huanyong Line has served as an important indicator of inequality in China. Similarly, this North-South division line is expected to reveal inequalities in global development and could be linked to relevant indicators of the SDGs.

Limitations of the study

The research of global urban development has limitations in the following two aspects. First, it fails to conduct a detailed analysis in conjunction with setting development scenarios within urban areas. Although NTL data provide long-term urban measures at multiple scales, it cannot acquire the spatial layout and urban structure in built-up areas and evaluate their potential influences on urban development. It is not conducive to explaining how cities with different urban development patterns evolve individually. Second, this study lacks effective models to quantitatively simulate and predict potential variations and trends of global urban development in multiple temporal scales. Although we could roughly infer its possible changes by combining with information such as population and economic growth, it is difficult to provide accurate judgments on how urban development changes under different projected scenarios. Hence, how to couple the development situations within urban areas and establish quantitative models to forecast urban development are problems that need to be addressed in future research.

STAR★METHODS

Detailed methods are provided in the online version of this paper and include the following:

- KEY RESOURCES TABLE
- RESOURCE AVAILABILITY
  - Lead contact
  - Materials availability
  - Data and code availability
- METHOD DETAILS
  - Generating time series of NTL-derived urban measures
  - The shape-based clustering method
  - The reclassification of urban development patterns
- QUANTIFICATION AND STATISTICAL ANALYSIS

SUPPLEMENTAL INFORMATION

Supplemental information can be found online at https://doi.org/10.1016/j.isci.2021.102729.

ACKNOWLEDGMENTS

This study was supported by the National Key R&D Program of China (No. 2017YFA0604402), National Natural Science Foundation of China (No. 41801306), National Key R&D Program of China (No. 2019YFB2103104).

AUTHOR CONTRIBUTIONS

X.L. and Y.T.Z. designed the research; Y.T.Z. performed the experiments, drafted and revised the manuscript; Y.T.Z, X.L., K.H., S.J.W., H.F.Z. and Y.Y. amended the manuscript; Y.Y. provided technical supports; Q.Q.L., W.T., H.Z., K.S.F., and L.X.S. contributed to the improvement of the manuscript.

DECLARATION OF INTERESTS

The authors declare no competing interests.

Received: December 16, 2019
Revised: April 26, 2021
Accepted: June 10, 2021
Published: July 23, 2021

REFERENCES

Acuto, M., and Parnell, S. (2016). Leave no city behind. Science *352*, 873.

Acuto, M., Parnell, S., and Seto, K.C. (2018). Building a global urban science. Nat. Sustain. *1*, 2–4.

Antrop, M. (2004). Landscape change and the urbanization process in Europe. Landscape Urban Plan *67*, 9–26.

Bagan, H., and Yamagata, Y. (2015). Analysis of urban growth and estimating population density using satellite images of nighttime lights and land-use and population data. Gisci. Remote Sens. *52*, 765–780.

Bagan, H., and Yamagata, Y. (2012). Landsat analysis of urban growth: how Tokyo became the world's largest megacity during the last 40 years. Remote Sens. Environ. *127*, 210–222.

Bagnall, A., and Janacek, G. (2005). Clustering time series with clipped data. Mach. Learn. *58*, 151–178.

Ban, Y., Jacob, A., and Gamba, P. (2015). Spaceborne SAR data for global urban mapping at 30 m resolution using a robust urban extractor. ISPRS J. Photogramm. *103*, 28–37.

Berndt, D.J., and Clifford, J. (1994). Using dynamic time warping to find patterns in time series. In KDD Workshop, pp. 359–370.

Bloom, D.E., Canning, D., and Lubet, A. (2015). Global population aging: facts, challenges, solutions & perspectives. Daedalus *144*, 80–92.

Bosworth, B., and Collins, S.M. (2008). Accounting for growth: comparing China and India. J. Econ. Perspect. *22*, 45–66.

Buhaug, H., and Urdal, H. (2013). An urbanization bomb? Population growth and social disorder in cities. Glob. Environ. Change *23*, 1–10.

Chen, D., Zhang, Y., Yao, Y., Hong, Y., Guan, Q., and Tu, W. (2019a). Exploring the spatial differentiation of urbanization on two sides of the Hu Huanyong Line–based on nighttime light data and cellular automata. Appl. Geogr. *112*, 102081.

Chen, Z., Yu, B., Zhou, Y., Liu, H., Yang, C., Shi, K., and Wu, J. (2019b). Mapping global Urban areas from 2000 to 2012 using time-series nighttime light data and MODIS products. IEEE J. STARS *12*, 1143–1153.

Cheshire, P. (1995). A new phase of urban development in Western Europe? The evidence for the 1980s. Urban Stud. *32*, 1045–1063.

Cohen, B. (2006). Urbanization in developing countries: current trends, future projections, and key challenges for sustainability. Technol. Soc. *28*, 63–80.

Cohen, B. (2004). Urban growth in developing countries: a review of current trends and a caution regarding existing forecasts. World Dev. *32*, 23–51.

Connolly, C. (2019). Worlding cities through transportation infrastructure. Environ. Plann. A: Economy Space *51*, 617–635.

Dellink, R., Chateau, J., Lanzi, E., and Magn E, B. (2017). Long-term economic growth projections in the shared socioeconomic pathways. Glob. Environ. Change *42*, 200–214.

Eckert, S., and Kohler, S. (2014). Urbanization and health in developing countries: a systematic review. World Health Popul. *15*, 7–20.

Elvidge, C.D. (2014), Global Urban Monitoring and Assessment Through Earth Observation, Q. Weng, ed. (the CRC Press), pp. 97–118.

Elvidge, C.D., Ziskin, D., Baugh, K.E., Tuttle, B.T., Ghosh, T., Pack, D.W., Erwin, E.H., and Zhizhin, M. (2009). A fifteen year record of global natural gas flaring derived from satellite data. Energies *2*, 595–622.

Esch, T., Heldens, W., Hirner, A., Keil, M., Marconcini, M., Roth, A., Zeidler, J., Dech, S., and Strano, E. (2017). Breaking new ground in mapping human settlements from space–The Global Urban Footprint. ISPRS J. Photogramm. *134*, 30–42.

Far I As, I., and Bender, T. (2012). Urban Assemblages: How Actor-Network Theory Changes Urban Studies (Routledge).

Fernandes, N. (2020). Economic Effects of Coronavirus Outbreak (COVID-19) on the World Economy (IESE Business School). .Working Paper No. WP-1240-E, Available at SSRN. https://doi.org/10.2139/ssrn.3557504. https://ssrn.com/abstract=3557504.

Getis, A. (2010). Spatial autocorrelation. In Handbook of Applied Spatial Analysis, M.M. Fischer and A. Getis, eds. (Springer), pp. 255–278.

Global Administrative Areas (2015). GADM Database of Global Administrative Areas (Version 2.8) (Global Administrative Areas). http://www.gadm.org/.

Gong, P., Wang, J., Yu, L., Zhao, Y., Zhao, Y., Liang, L., Niu, Z., Huang, X., Fu, H., Liu, S., et al. (2013). Finer resolution observation and monitoring of global land cover: first mapping results with Landsat TM and ETM+ data. Int. J. Remote Sens. *34*, 2607–2654.

Higo, M., and Khan, H.T. (2015). Global population aging: Unequal distribution of risks in later life between developed and developing countries. Glob. Soc. Pol. *15*, 146–166.

Jokar Arsanjani, J. (2019). Characterizing and monitoring global landscapes using GlobeLand30 datasets: the first decade of the twenty-first century. Int. J. Digit. Earth *12*, 642–660.

Jones, B., and O Neill, B.C. (2016). Spatially explicit global population scenarios consistent with the Shared Socioeconomic Pathways. Environ. Res. Lett. *11*, 84003.

Judt, T. (2006). Postwar: a history of Europe since 1945. Foreign Aff. *84*, 159.

Le Quere, C., Jackson, R.B., Jones, M.W., Smith, A.J., Abernethy, S., Andrew, R.M., De-Gol, A.J., Willis, D.R., Shan, Y., Canadell, J.G., et al. (2020). Temporary reduction in daily global CO^2 emissions during the COVID-19 forced confinement. Nat. Clim. Change, 1–7.

Li, X., Chen, G., Liu, X., Liang, X., Wang, S., Chen, Y., Pei, F., and Xu, X. (2017a). A new global land-use and land-cover change product at a 1-km resolution for 2010 to 2100 based on human-environment interactions. Ann. Am. Assoc. Geogr. 1–20.

Li, X., Li, D., Xu, H., and Wu, C. (2017b). Intercalibration between DMSP/OLS and VIIRS night-time light images to evaluate city light dynamics of Syria's major human settlement during Syrian Civil War. Int. J. Remote Sens. *38*, 5934–5951.

Li, X., and Zhou, Y. (2017). Urban mapping using DMSP/OLS stable night-time light: a review. Int. J. Remote Sens. 1–17.

Liu, Z., He, C., Zhang, Q., Huang, Q., and Yang, Y. (2012). Extracting the dynamics of urban expansion in China using DMSP-OLS nighttime light data from 1992 to 2008. Landscape Urban Plan *106*, 62–72.

Lloyd, R. (2012). Urbanization and the southern United States. Annu. Rev. Sociol. *38*, 483–506.

Ma, T., Zhou, C., Pei, T., Haynie, S., and Fan, J. (2012). Quantitative estimation of urbanization dynamics using time series of DMSP/OLS nighttime light data: a comparative case study from China's cities. Remote Sens. Environ. *124*, 99–107.

Maddison, A. (1983). A comparison of levels of GDP per capita in developed and developing countries, 1700-1980. J. Econ. Hist. 27–41.

McDonald, R.I., Marcotullio, P.J., and G U Neralp, B. (2013). Urbanization and global trends in biodiversity and ecosystem services. In Urbanization, Biodiversity and Ecosystem Services: Challenges and Opportunities, T. Elmqvist, M. Fragkias, J. Goodness, B. Güneralp, P.J. Marcotullio, R.I. McDonald, S. Parnell, M. Schewenius, M. Sendstad, and K.C. Seto, et al., eds. (Springer), pp. 31–52.

McFarlane, C. (2011). Assemblage and critical urbanism. City *15*, 204–224.

Merrifield, A. (2013). The urban question under planetary urbanization. Int. J. Urban Reg. Res. *37*, 909–922.

Messinis, G. (2015). Which comes first-urbanization or economic growth? Evidence from heterogeneous panel causality tests. Appl. Econ. Lett. *22*, 349–355.

Mirkin, B. (2005). Clustering for Data Mining: A Data Recovery Approach (Chapman & Hall/CRC), pp. 109–110.

NASA, L.D. (2016). MODIS/Terra Land Water Mask Derived from MODIS and SRTM L3 Global 250m Grid (MOD44W) (NASA EOSDIS Land Processes DAAC, USGS Earth Resources Observation and Science (EROS) Center). https://lpdaac.usgs.gov.

O'Neill, B.C., Dalton, M., Fuchs, R., Jiang, L., Pachauri, S., and Zigova, K. (2010). Global demographic trends and future carbon emissions. Proc. Natl. Acad. Sci. U S A *107*, 17521–17526.

Oswin, N. (2018). Planetary urbanization: a view from outside. Environ. Plann. D Soc. Space *36*, 540–546.

Pandit, K. (1997). The southern migration turnaround and current patterns. Southeast. Geographer. *37*, 238–250.

Parnell, S. (2016). Defining a global urban development agenda. World Dev. *78*, 529–540.

Petitjean, F.C.C.O., Ketterlin, A., and Gan C C Arski, P. (2011). A global averaging method for dynamic time warping, with applications to clustering. Pattern Recogn. *44*, 678–693.

Proville, J., Zavala-Araiza, D., and Wagner, G. (2017). Night-time lights: a global, long term look at links to socio-economic trends. PLoS One *12*, e174610.

Robinson, J. (2011). Cities in a world of cities: the comparative gesture. Int. J. Urban Reg. Res. *35*, 1–23.

Robinson, J. (2016). Thinking cities through elsewhere: comparative tactics for a more global urban studies. Prog. Hum. Geogr. *40*, 3–29.

Rousseeuw, P.J. (1987). Silhouettes: a graphical aid to the interpretation and validation of cluster analysis. J. Comput. Appl. Math. *20*, 53–65.

Roy, A., and Ong, A. (2011). Worlding Cities: Asian Experiments and the Art of Being Global (John Wiley & Sons).

Sankhe, S., Vittal, I., and Mohan, A. (2011). Urban giants: India and China, and their urbanization paths. Environ. Urban. Asia *2*, 1–12.

Schneider, A., Friedl, M.A., and Potere, D. (2009). A new map of global urban extent from MODIS satellite data. Environ. Res. Lett. *4*, 44003.

Seto, K.C., Fragkias, M., G U Neralp, B., and Reilly, M.K. (2011). A meta-analysis of global urban land expansion. PLoS One *6*, e23777.

Sharma, R.C., Tateishi, R., Hara, K., Gharechelou, S., and Iizuka, K. (2016). Global mapping of urban built-up areas of year 2014 by combining MODIS multispectral data with VIIRS nighttime light data. Int. J. Digit. Earth *9*, 1004–1020.

Small, C., Elvidge, C.D., Balk, D., and Montgomery, M. (2011). Spatial scaling of stable night lights. Remote Sens. Environ. *115*, 269–280.

Sutton, P., Roberts, D., Elvidge, C., and Baugh, K. (2001). Census from Heaven: an estimate of the global human population using night-time satellite imagery. Int. J. Remote Sens. *22*, 3061–3076.

Therien, J. (1999). Beyond the North-South divide: the two tales of world poverty. Third World Q. *20*, 723–742.

Turok, I., and Mykhnenko, V. (2007). The trajectories of European cities, 1960–2005. Cities *24*, 165–182.

UN DESA. (2018). World Urbanization Prospects: The 2018 Revision (United Nations Department of Economics and Social Affairs, Population Division).

Wang, H., He, Q., Liu, X., Zhuang, Y., and Hong, S. (2012). Global urbanization research from 1991 to 2009: a systematic research review. Landscape Urban Plan *104*, 299–309.

Yu, B., Deng, S., Liu, G., Yang, C., Chen, Z., Hill, C.J., and Wu, J. (2018). Nighttime light images reveal spatial-temporal dynamics of global anthropogenic resources accumulation above ground. Environ. Sci. Technol. *52*, 11520–11527.

Zhang, Q., and Seto, K.C. (2011). Mapping urbanization dynamics at regional and global scales using multi-temporal DMSP/OLS nighttime light data. Remote Sens. Environ. *115*, 2320–2329.

Zhou, Y., Li, X., Asrar, G.R., Smith, S.J., and Imhoff, M. (2018). A global record of annual urban dynamics (1992–2013) from nighttime lights. Remote Sens. Environ. *219*, 206–220.

Zhou, Y., Smith, S.J., Elvidge, C.D., Zhao, K., Thomson, A., and Imhoff, M. (2014). A cluster-based method to map urban area from DMSP/OLS nightlights. Remote Sens. Environ. *147*, 173–185.

Zhou, Y., Smith, S.J., Zhao, K., Imhoff, M., Thomson, A., Bond-Lamberty, B., Asrar, G.R., Zhang, X., He, C., and Elvidge, C.D. (2015). A global map of urban extent from nightlights. Environ. Res. Lett. *10*, 54011.

STAR★METHODS

KEY RESOURCES TABLE

REAGENT or RESOURCE	SOURCE	IDENTIFIER
Deposited data		
DMSP/OLS nighttime light data	NOAA	https://www.ngdc.noaa.gov/eog/dmsp/downloadV4composites.html
NPP/VIIRS nighttime light data	NOAA	https://www.ngdc.noaa.gov/eog/viirs/download_ut_mos.html
Global administrative areas data	GADM	http://www.gadm.org/
Global socioeconomic factors	World bank	https://data.worldbank.org/
Chinese socioeconomic factors	China national knowledge infrastructure	http://data.cnki.net/
Software and algorithms		
ArcGIS	ESRI	https://www.arcgis.com/index.html
QGIS	Open-source software	https://qgis.org/en/site/

RESOURCE AVAILABILITY

Lead contact

Further information and requests for data and code should be directed to and will be fulfilled by the lead contact, Xia Li (lixia@geo.ecnu.edu.cn).

Materials availability

This study did not generate new materials.

Data and code availability

The data used in this study are all available from public resources that have been appropriately cited within the manuscript. Besides, the data and code can also be obtained from the lead contact. Here, the websites to acquire these datasets are also listed as follows: DMSP/OLS nighttime light data (https://www.ngdc.noaa.gov/eog/dmsp/downloadV4composites.html); NPP/VIIRS nighttime light data (https://www.ngdc.noaa.gov/eog/viirs/download_ut_mos.html); Global administrative areas data (http://www.gadm.org/); Global socioeconomic factors (https://data.worldbank.org/); Chinese socioeconomic factors (http://data.cnki.net/).

METHOD DETAILS

Generating time series of NTL-derived urban measures

NTL data got from the Operational Line-scan System of the Defense Meteorological Satellite Program (DMSP/OLS, 1992-2013) and the Visible Infrared Imaging Radiometer Suite onboard the National Polar-orbiting Partnership satellites (NPP/VIIRS, 2012-2018) were processed to generate time-series NTL-derived urban measures at the country, region and city scales during the period of 1992-2018 (Chen et al., 2019a; Elvidge et al., 2014). Considering that there exist huge differences in DMSP/OLS and NPP/VIIRS NTL data on the spatiotemporal resolution, spectral response, overpass time, variance range and onboard calibration (Li et al., 2017b), two kinds of images were intercalibrated to produce good-quality NTL-derived urban measures, respectively.

For DMSP/OLS data, in order to eliminate nighttime light intensity deviations caused by some unavoidable factors, such as light on water surfaces, natural gas flaring and light on non-urban areas, masks made by the MODIS land-water product (NASA, 2016), gas flare data (Elvidge et al., 2009) and a threshold method between urban and non-urban areas (Small et al., 2011), were utilized to remove noisy light. Then, we implemented an inter-calibration of the annual composites to offset the defects caused by the lack of on-board

calibration in OLS sensors through Equation 1 (Elvidge et al., 2009, 2014). $DN_{calibrated}$ and DN are pixel's digital number after and before the intercalibration, respectively; C_0, C_1, C_2 are coefficients determined by the quadratic equation regression model shown in Table S3 for each OLS sensor. An example of NTL amount comparison in China before and after the intercalibration shows that the intercalibration makes time-series NTL data smooth and consistent among sensors in the same and different years (Figure S2). Afterward, an intra-annual composition was used to remove noisy light pixels (Liu et al., 2012).

$$DN_{calibrated} = C_0 + C_1 * DN + C_2 * DN^2 \quad \text{(Equation 1)}$$

For NPP/VIIRS data, monthly products were merged into annual products by averaging pixel values within each year, such as from Apr. to Dec. in 2012 and from Jan. to Dec. in 2018; then six separate image tiles in one year were used to mosaic a whole image of this year, and seven VIIRS NTL images from 2012 to 2018 in total could be produced. For each annual NTL image, the bilinear method was used to resample the image to produce a new image that had the same spatial resolution as DMSP/OLS data. Considering that NPP/VIIRS can detect low-level light that DMSP/OLS fails, each pixel in NPP/VIIRS was subtracted by 0.3 nW cm^{-2} sr^{-1} to eliminate the influence (Chen et al., 2019a). After that, an intercalibration model was built to ensure the temporal correspondence between NPP/VIIRS and DMSP/OLS data based on the overlapped years, i.e., 2012 and 2013 (Li et al., 2017b). In Equation 2, $\boldsymbol{Y}$ and $\boldsymbol{X}$ represent DMSP/OLS and NPP/VIIRS data; $G(\bullet)$ is the power function for matrix transformation; $\boldsymbol{M}$ is a low pass filter to smooth the NTL image with a window size of θ and a standard deviation of Gaussian distribution of σ; "$*$" refers to their spatial covolution; a and b are coefficients.

$$\boldsymbol{Y} = aG(\boldsymbol{X}, b) * \boldsymbol{M}_{(\theta,\sigma)} \quad \text{(Equation 2)}$$

In this study, the window size of θ was set as 13, and other coefficients were estimated by the global search algorithm (Chen et al., 2019a; Li et al., 2017b). Notice that we utilized GlobCover 2009, one global landcover product released by European Space Agency, to extract urban areas of NPP/VIIRS in 2012 and 2013 as the train and validation data in Equation 2. Finally, the values of a, b and were 35.2989, 0.1633 and 0.4891 respectively. The comparisons of Pearson's R and the root-mean-square error (RMSE) between the original and intercalibrated images reflect the effectiveness of this intercalibration model (Table S4). Afterward, this model was used to intercalibrate NPP/VIIRS images from 2014 to 2018 when some noises were removed, such as light on water surfaces, light from gas flaring and other sources, etc. Then, we utilized two thresholds to avoid the influence of non-urban areas' light by setting the threshold as 13 (pixel's value below 13 was set as 0), and avoid the saturation effect by setting the threshold as 60 (pixel's value above 60 was set as 60).

The primary units at the country, region and city scales were extracted based on the Global Administrative Areas dataset (GADM) (Global Administrative Areas, 2015). Especially, due to the fact that different countries and regions hold different administrative division settings, the region scale is defined as an intermediate scale between the country and city scales (e.g., provinces in China and states in the United States). After converting NTL images into Mollweide equal-area projection (Elvidge et al., 2009), we calculated the weighted light area in each unit as the NTL-derived urban measure at three scales. The weighted light area of one pixel is defined as the product of its area and the normalized DN value, and the weighted light area of one unit is the sum of all pixels' weighted light area within it, expressed in Equation 3, where $WLA_{(i,j)}$ represents the weighted light area of the j unit in the i year; $DN'_{(i,j,p)}$ is the normalized DN value of the p pixel of the j unit in the i year; $S_{(i,j,p)}$ is the area of the p pixel of the j unit in the i year (Ma et al., 2012).

$$WLA_{(i,j)} = \sum_{p} DN'_{(i,j,p)} * S_{(i,j,p)} \quad \text{(Equation 3)}$$

Then, the weighted light areas were grouped in sequence from 1992 to 2018 to generate time-series NTL vectors. In order to further ensure the correspondence of DMSP/OLS and NPP/VIIRS data, an adjustment coefficient γ (the ratio of the weighted light area of DMSP/OLS in 2013 to that of NPP/VIIRS in 2013) was multiplied by the weighted light area from 2014 to 2018 to obtain more consistent time-series NTL vectors. Then, the exponential smoothing algorithm with the smoothing factor of 0.1 was used to eliminate the influence of noises and emphasize the overall variations of time-series NTL vectors during the period of 1992-2018. Notice that some units had extremely low NTL-derived urban measures, where the weighted light area of certain years was zero. All of these units are defined as "Excluded Area", which are excluded from the calculations in this paper, including the clustering, Moran's I and classification. After these processes, the available instances at the country, region, and city scales are 221, 2,649, and 24,933 respectively.

The shape-based clustering method

A shape-based clustering framework was used to extract the temporal patterns of global urban development based on time-series NTL vectors, including shape measurement based on dynamic time warping (DTW), and the K-Medoids clustering method. First, DTW was utilized to measure the dissimilarities among time-series NTL vectors. Different from the Euclidean distance, DTW is one of the most widely used methods for shape similarity measurement, which can find the optimal global alignment among time series through dynamic programming formulation (Bagnall and Janacek, 2005; Berndt and Clifford, 1994). By this, the difference among time-series NTL vectors is more focused on shape patterns, which can benefit the extraction of the temporal patterns of urban development. Second, a K-Medoids clustering method using anomalous pattern (Mirkin, 2005) was adopted to detect the underlying centered shape patterns hidden behind the NTL time series based on the DTW-based distance (Bagnall and Janacek, 2005; Berndt and Clifford, 1994). Different from the K-Means, the K-Medoids method chooses an existing time-series NTL instance (the medoid of the cluster) as the clustering center rather than averaging all time-series NTL instances in the cluster, thus making the clustering process more operational in DTW-based similarity measures (Petitjean et al., 2011).

In order to select the best pattern centers, Silhouette was applied to estimate the clustering quality for the clustering results with various clustering number (Rousseeuw, 1987). At either scale, the clustering result with the highest Silhouette score was regarded as the best pattern extraction results. The shape pattern of its clustering center curve was the corresponding temporal pattern of urban development. To improve the computational effort at the city scale, about 20% of cities were chosen as the input of the clustering model, and other cities were classified through the DTW distance to the clustering centers. Importantly, to highlight the difference of shape patterns among time-series NTL vectors in the clustering method, each vector was standardized separately through the Z score standardization in Equation 4, where μ and σ are the average value and the standard deviation in each time-series NTL vector, respectively; λ_i and x_i are the standardized and original NTL-derived urban measures, respectively. Finally, in Figure 1, the temporal rising and declining patterns were endowed to depict the shape patterns of clustering center curves at the country, region and city scales.

$$\lambda_i = \frac{x_i - \mu}{\sigma} \quad \text{(Equation 4)}$$

The reclassification of urban development patterns

The change rate of the temporal rising and declining patterns could be depicted using a fitting method between the time-series NTL vectors and the function in Equation 5, where x and y represent the time and the value of NTL-derived urban measures respectively. Thus, with corresponding parameter domains, we can obtain the corresponding temporal patterns with different change rates, such as the accelerated rise ($b > 0, c > 1$), the accelerated decline ($b < 0, c > 1$), the decelerated rise ($b > 0, 0 < c < 1$), the decelerated decline ($b < 0, 0 < c < 1$), the uniform rise ($b > 0, c = 1$) and the uniform decline ($b < 0, c = 1$). In actual applications, the intervals of c are readjusted to 0.9 and 1.1 in the recognition of the uniform rise and decline patterns. The stable pattern is identified when the overall trend of time-series NTL vectors basically keeps constant with slight fluctuation.

$$y = a + b * x^c \ (x > 0) \quad \text{(Equation 5)}$$

However, due to large temporal variations and residual noises existing in NTL data (Zhang and Seto, 2011), it is inaccurate to judge its patterns only through the fitting method in Equation 5. Thus, for a city to be labeled, a nonlinear fitting between the time-series NTL vector and Equation 5 is initially executed to get an initial pattern result. Then, visual judgment is employed to decide its final pattern, by checking its overall trend, change rate, fluctuations, and its accordance with the seven patterns. During this process, a time-series NTL vector without the decline or rise trend is recognized as the stable pattern. However, this method is too onerous to label all the cities around the globe. Especially, the procedures involving manual justification are tedious and impractical.

Hence, we used a backpropagation neural network (BPNN) with three hidden layers to classify the patterns of urban development at the city scale. The input and output are the time-series NTL vectors and the seven patterns respectively. Of all the 24,933 cities at the city scale, 700 cities were chosen to label their patterns (100 cities per pattern) based on the above sample selection procedures. We then repeatedly run the BPNN classifier 100 times with different train and validate datasets, which are randomly split from the

labeled dataset. For each training process, 75% of labeled samples were randomly selected as a training dataset to train the BPNN classifier, and the remaining 25% was used to conduct an accuracy assessment. High performance of the BPNN algorithm was obtained, with the average overall accuracy and Kappa coefficient of 0.92 and 0.91 respectively. Finally, we utilized the well-trained classifier to classify the patterns of all the cities at the city scale.

QUANTIFICATION AND STATISTICAL ANALYSIS

In the shaped-based clustering, the medoid of each cluster refers to an actual vector of NTL-derived urban measures that minimizes a sum of pairwise DTW distances, i.e., the clustering center curve in Figure 1. The Global Moran's I was calculated in the spatial autocorrelation module in ArcGIS with a Euclidean distance band of 3,000,000. The calculation ignored the "Excluded Area" and obtained the Moran's I result with the confidence level of 99% at all three scales in Figure 1. It is worthy to note that the "Excluded Area" was determined by checking whether there was zero in the values of the weighted light area from 1992 to 2018, and then the result was inherited directly into the "Excluded Area" in Figures 1 and 2. In the box plots of Figure 4, the Line-North and Line-South attribution of each growth rate value was identified through the position of the research unit relative to the division line. Besides, some growth rate values in box plots were not visualized due to their high values compared to the majority in Figure 4.